

Investigation of Peritectic Behavior of Steel Using a Thermal Analysis Technique



SUNDAY ABRAHAM, RICK BODNAR, JOHAN LONNQVIST,
FATEMEH SHAHBAZIAN, ANDERS LAGERSTEDT, and MAGNUS ANDERSSON

During solidification, the peritectic reaction can occur in a wide range of materials, including ferrous and non-ferrous alloys. The kinetic and thermodynamic principles that govern the peritectic reaction in regard to solute diffusion and phase transformation are well understood, and the negative impact that the peritectic reaction has on the surface quality of as-cast steel products is well documented. In ferroalloys, the peritectic reaction occurs between the hypoperitectic (0.09 pct C) and hyperperitectic (0.53 pct C) regions of the iron-carbon phase diagram. Beside the carbon content, the magnitude of the peritectic reaction in a given steel is affected by the contents of other solute elements. However, our understanding of the effect of all dissolved elements on the peritectic reaction is still evolving. There are over a dozen equations that have been proposed for predicting the peritectic nature of steels. Some of these equations were developed for application to specific groups of steels, chemistries, and casting conditions. In this paper, the predictive power of four peritectic equations is compared to the results from thermal analysis experiments conducted on steels with varying concentrations of dissolved elements. Based on the thermal analysis results, an equation is proposed for calculating the latent heat of the peritectic reaction for a given solute element.

<https://doi.org/10.1007/s11661-019-05148-6>

© The Minerals, Metals & Materials Society and ASM International 2019

I. INTRODUCTION

DURING solidification, the peritectic reaction can occur in a wide variety of materials, including ferrous and non-ferrous alloys.^[1–10] The term peritectic reaction is derived from the fact that during solidification a secondary phase grows peripherally on the primary phase. This distinct solidification phenomenon occurs at certain composition ranges where both the primary and secondary phases coexist for some time. The difference between the thermal coefficient of contraction of the primary and secondary phases makes peritectic steels challenging to cast. In Fe-C alloys, the peritectic reaction occurs over a carbon range of 0.09 to 0.53 pct.^[11,12] These two extreme ends of the peritectic range are referred to as the hypoperitectic and hyperperitectic points, respectively. However, peritectic

reactions are described by some researchers as occurring mostly between a tighter range of carbon contents, for example, 0.080 to 0.180 pct. The hypoperitectic and hyperperitectic points for given steel will change depending on the concentrations of other dissolved solute elements. In the “peritectic” range, once a certain temperature is reached, part of the primary phase (delta ferrite) that precipitated from the liquid reacts with the residual melt to form a secondary phase (austenite). The austenite precipitates around the remaining delta ferrite, preventing its access to the remaining liquid. The austenite then begins to grow inward into the delta ferrite and outward into the liquid. The transformation to austenite takes some time to finish and hence, the peritectic reaction itself refers to the initial precipitation of austenite on the periphery of the delta ferrite. The gradual transformation of delta ferrite to austenite at lower temperatures is referred to as a peritectic transformation.^[13] The peritectic reaction and transformation during solidification are illustrated in Figure 1.^[14–16] It should be noted that in certain cases, the secondary phase, austenite, may nucleate in the liquid in lieu of an existing primary phase, delta ferrite.

Due to the tighter atomic packing of the austenite (FCC structure) compared to the delta ferrite (BCC structure) during the peritectic reaction, the volume of austenite contracts more than the delta ferrite.^[17] This difference in the thermal contraction of the two phases

SUNDAY ABRAHAM and RICK BODNAR are with the SSAB Americas, 1755 Bill Sharp Boulevard, Muscatine, IA 52761. Contact e-mail: Sunday.Abraham@ssab.com JOHAN LONNQVIST and FATEMEH SHAHBAZIAN are with the Swerim, Isafjordsgatan 28A, 164 40 Kista, Sweden. ANDERS LAGERSTEDT and MAGNUS ANDERSSON are with the SSAB Oxelösund AB, 80 Oxelösund SE613, Oxelösund, Sweden.

Manuscript submitted September 8, 2018.

Article published online February 19, 2019

makes peritectic steel prone to cracking, particularly longitudinal cracking during solidification.^[18] As a result, some steelmakers attempt to avoid casting peritectic steels, and others take steps to avoid peritectic-related defects in the as-cast product. These measures include chemistry modifications, casting at slower speeds, application of mold powder with moderate heat transfer rate, maintaining moderate superheat, and ensuring an optimal flow pattern in the mold. Hence, it is important for steelmakers to understand how different alloying elements affect the peritectic reaction. This will ensure that adequate measures can be taken during casting to minimize the impact on the surface quality of as-cast products.

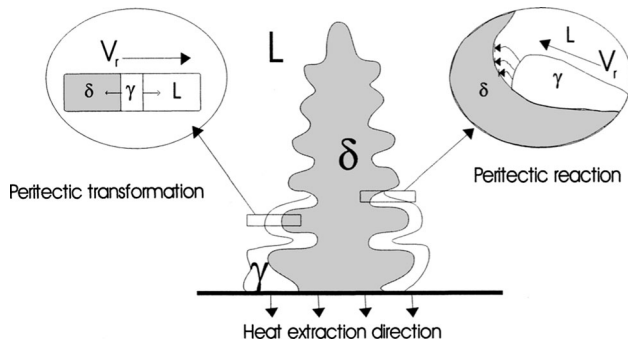


Fig. 1—Mechanism of peritectic solidification (Reprinted from Ref. [15], with permission).

Various methods have been employed to study the peritectic reaction, including simulation and modeling,^[14–16,19–23] and *in-situ* observation of the peritectic reaction during solidification in a confocal laser scanning microscope.^[24–29] In addition, over a dozen equations have been proposed for determining peritectic behavior in Fe-C systems. The first sets of equations proposed for the peritectic prediction were those of Ishida *et al.*,^[30,31] and Yasumoto *et al.*^[30,32] These equations only considered the effects of C, Mn, Si, and S. Subsequent equations for peritectic indexing included the effects of more solute elements.^[33] In this paper, the equations proposed by Kagawa and Okamoto,^[34] Wolf,^[12] Blazek *et al.*,^[35] and Abraham^[36] are used to determine the peritectic nature of steel of different chemistries. The predictive power of these equations is compared to the results of thermal analysis experiments conducted according to the procedure employed in the work of Carlsson and Callmer,^[37] and others.^[15,38,39] Two steel grades, one peritectic and the other non-peritectic, were chosen for the study. The steel grades used in this study have carbon contents ranging from 0.05 to 0.17 pct. In addition to C, the effects of Si, Cr, and Mo on the peritectic reaction were investigated.

II. EXPERIMENTAL

The thermal analysis experimental set-up, which is shown in Figure 2 left, comprises of a high-frequency induction furnace with a data logging system. The crucible is densely sintered alumina in which a 0.080 kg

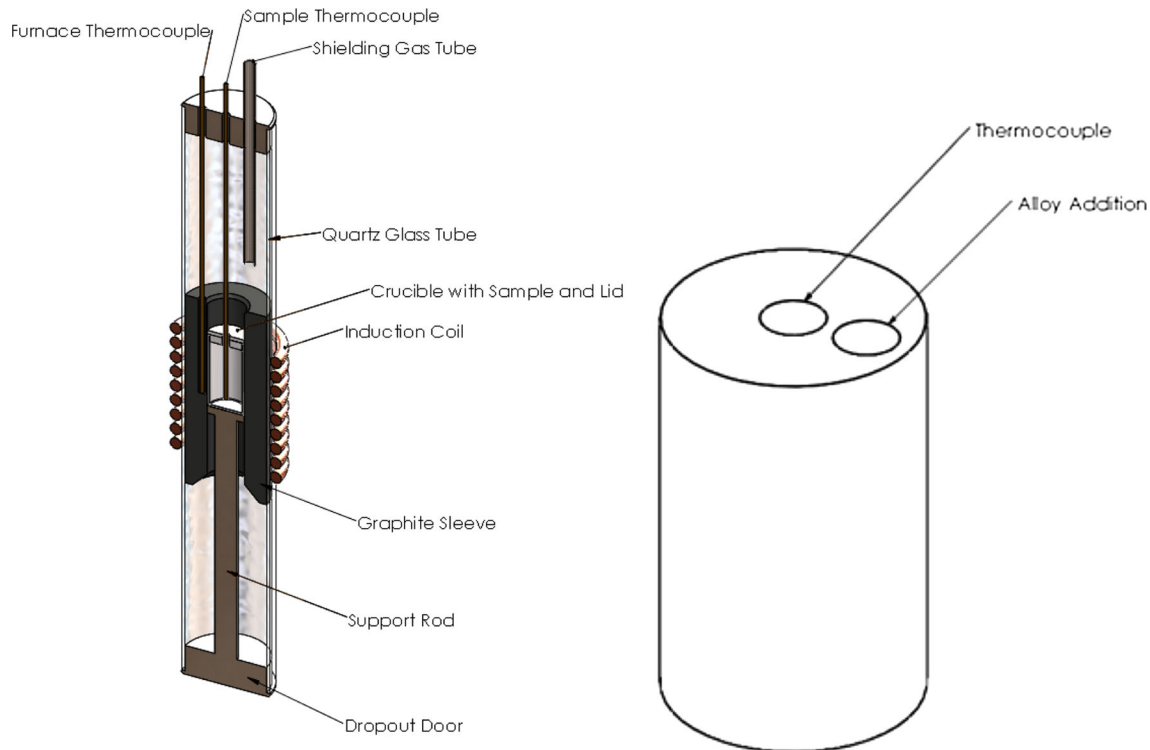


Fig. 2—Schematic diagram of experimental set-up (left) and schematic diagram of specimens and locations for thermocouple and alloy addition (right).

sample was placed. The sample was kept relatively small in order to eliminate the effect of a thermal gradient on the liquidus and solidus temperatures.

The crucible was located in the center of a graphite cylinder heated by an induction coil. The furnace temperature was measured using a 1-mm-diameter alumina-shielded-type S thermocouple inserted along the induction field lines to minimize any interference from the magnetic field. The temperature measured in the graphite ring was also the temperature used to control the furnace *via* a Proportional-Integral-Derivative (PID) regulator. Another recording thermocouple was placed in the crucible to measure the sample temperature. This set-up makes the sample passive and enables an estimation of heat evolution based on the temperature difference between the sample and the crucible. The whole set-up was enclosed in a quartz tube flushed with argon as a protective atmosphere. At any time during the experiment, the dropout door could be opened and the sample quenched in a bucket of water located under the furnace chamber. Both the sample and the furnace temperatures were logged at 10 Hz (10 measurements per second) together with the set temperature, runtime, and power of the induction generator as a function of time. The capacity of the induction generator is 20 kW, but only a small fraction of the power was used during the experiments.

Since the samples must be melted first before cooling to the point of peritectic reaction, alloying elements were added to the samples in order to study the effects of varying concentrations of elements on the peritectic reaction. The amounts of alloying elements that were added to achieve the required concentrations were calculated using a mass balance analysis. Alloying elements were added into a hole drilled in the sample,

as shown in Figure 2 right. The samples were 40-mm-long cylinders, 25 mm in diameter. The composition of the sample was varied using the four cited peritectic equations as a guideline. The concentrations of elements in the samples were verified after thermal analysis by performing chemical analysis using OES (optical emission spectroscopy) and Leco (combustion infrared) instruments. Leco instruments were used to analyze N, S, and C contents, while the balance of the elements were determined using the OES technique.

Cooling rates of 0.1 and 1.5 °C/s were investigated during solidification of each sample and duplicate thermal analysis experiments were conducted per sample per cooling rate. The error in cooling rate calculation was approximately ± 0.001 °C/s.

III. RESULTS AND ANALYSIS

The work of Carlsson and Callmer^[37] clearly describes the basic principles for identifying critical events using the temperature-time curve during solidification of steel as illustrated in Figure 3. The furnace and the molten sample are subjected to a constant cooling rate, but when the sample starts to solidify, the latent heat liberated decreases the cooling rate of the sample. In addition, since all reactions and transformations during the solidification process are accompanied by latent heat, the cooling rate of the sample decreases during each of these events. Hence, the derivative of the sample temperature *vs* time curve (dT/dt) provides useful information with respect to the occurrence of each of these events. This approach was employed to determine the start and end of the peritectic reaction for the steels investigated. The height of the peak of the dT/dt *vs* time

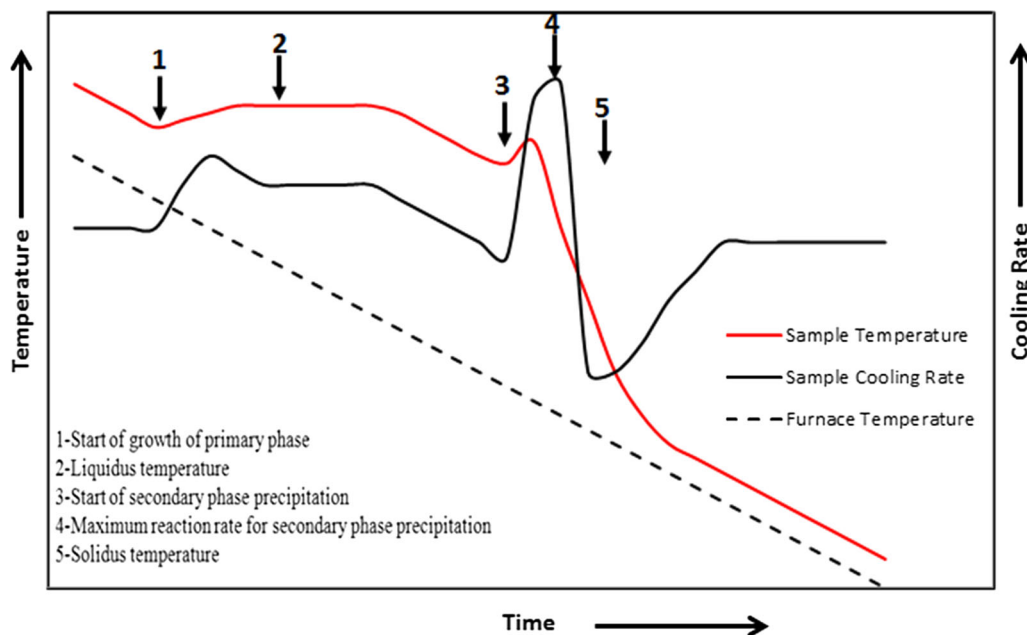


Fig. 3—Hypothetical temperature-time curve during solidification of peritectic steel.

curve at the time of the peritectic reaction represents the maximum reaction rate and is indicative of the magnitude of the peritectic reaction.

However, the primary data from the thermocouple signal based on the data logger were affected by interference from the magnetic field in addition to normal random variations of a thermocouple signal. This interference needed to be removed in order to evaluate the cooling rate in the form of the derivative of the temperature with respect to time. The technique chosen was a floating average calculated as

$$T_i = \frac{1}{N+1} \sum_{j=i-N}^{j=i+N} T_j, \quad [1]$$

where N is an arbitrary but sufficiently large number to achieve the necessary curve smoothing (for 1.5 °C/s it was about 20, and for 0.1 °C/s it was about 50).

The chemistries of the samples used in the experiments are shown in Table I. In Table I, NP is non-peritectic; while P is peritectic; “+” means increased content and “-” means decreased content.

A. Peritectic Steel vs Non-peritectic Steel

A summary of peritectic calculations for the peritectic and non-peritectic steels used in this study is provided in Table II. All of the peritectic equations are in agreement with respect to the peritectic nature of the two steels. For the peritectic steel, the carbon content is well within the peritectic ranges per both Kagawa and Okamoto's and Blazek *et al.*'s equations. According to Wolf's and Abraham's equations, the steel is within the peritectic ranges based on the ferrite potential index and peritectic

potential index, respectively. For the non-peritectic steel, all of the equations predict that the chemistry is non-peritectic. The carbon content is well outside the peritectic range per the Kagawa and Okamoto's equations. According to Blazek *et al.*'s equations, the carbon content is just above the upper peritectic value. According to Wolf's equations, the steel has a ferrite potential below the lower limit for peritectic steel, and according to Abraham's equations, the steel is below the lower limit of peritectic potential index. Thermal analysis results show that the peritectic steel exhibited a pronounced peritectic behavior (Figure 4(a)) and the non-peritectic steel exhibited a very mild peritectic behavior based on the change in the sample cooling rate during solidification. In Figures 4(a) and (b), the furnace temperature curves are provided as examples. The furnace temperature curves will be excluded from subsequent figures.

B. Non-peritectic Steel and Its Modifications to Peritectic Chemistries

1. Thermal analysis of sample NP

Thermal analysis results for NP at cooling rates of 0.1 and 1.5 °C/s are shown in Figures 5(a) and (b). Both results show only small changes in sample cooling rates, indicating that the steel is only mildly peritectic.

2. Thermal analysis of sample NP + Mo

The Mo content of the sample was increased from 0.051 to 0.601 pct. According to predictions by all of the peritectic equations, the modified chemistry is peritectic (Table III). Thermal analysis results show that the steel did exhibit significant peritectic behavior during

Table I. Chemistries of Samples Used for the Thermal Analysis Experiments, Weight Percent

Sample	C	Si	Mn	Cr	Ni	Mo	V	Ti	Cu
NP	0.169	0.195	0.933	0.204	0.134	0.051	0.022	0.011	0.284
NP + Mo	0.166	0.196	0.913	0.202	0.130	0.601	0.022	0.011	0.277
NP + Si	0.177	0.508	0.929	0.204	0.131	0.047	0.022	0.012	0.280
NP + Cr	0.163	0.196	0.929	0.805	0.131	0.047	0.023	0.010	0.278
P	0.130	0.343	1.209	0.267	0.089	0.156	0.032	0.014	0.192
P + Mo	0.126	0.324	1.177	0.258	0.087	1.883	0.032	0.013	0.189
P - Si	0.130	0.012	1.242	0.261	0.108	0.156	0.027	0.010	0.193
P - Cr	0.127	0.319	1.210	0.019	0.108	0.154	0.027	0.007	0.191
P-Si-Cr	0.117	0.093	1.082	0.106	0.101	0.049	0.024	0.005	0.178

Table II. Peritectic Calculations for Samples P and NP

Sample	Kagawa and Okamoto		Blazek <i>et al.</i>		Wolf		Abraham	
	C Range (Pct)	Peritectic (Y/N)	C Range (Pct)	Peritectic (Y/N)	Ferrite Potential Index	Peritectic (Y/N)	Peritectic Potential Index	Peritectic (Y/N)
P	0.098 to 0.198	Y	0.064 to 0.161	Y	0.95	Y	87	Y
NP	0.080 to 0.154	N	0.067 to 0.164	N	0.80	N	62	N

solidification based on the change in sample cooling rate (Figures 6(a) and (b)).

3. Thermal analysis of sample NP + Si

The chemistry of the sample was changed by increasing its Si content from 0.195 to 0.508 pct. All of the peritectic equations, except those of Blazek *et al.*, show that the steel is peritectic (Table IV). Thermal analysis results show that the steel exhibited peritectic behavior based on the change in sample cooling rate (Figures 7(a) and (b)).

4. Thermal analysis of sample NP + Cr

The chemistry of the sample was changed by increasing its Cr content from 0.20 to 0.80 pct. According to the predictions by all of the peritectic equations, the addition of Cr to the steel makes the steel peritectic (Table V). Thermal analysis results show that the steel indeed exhibited a significant peritectic behavior during solidification based on the change in sample cooling rate

of the samples (Figures 8(a) and (b)). The two thermal analysis experiments conducted at a cooling rate of 0.1 °C/s show a significant change in sample cooling rate, while one of the two experiments at a cooling of 1.5 °C/s shows a significant change in sample cooling rate compared to the sample with lower Cr content. The smaller change in sample cooling rate for the second sample at 1.5 °C/s could be a result of poor contact of the sample with the thermocouple.

C. Peritectic Steel and Its Modifications to Non-peritectic Chemistries

1. Thermal analysis of sample P

Thermal analysis results on the P sample at cooling rates of 0.1 and 1.5 °C/s show that the steel exhibits strong peritectic behavior during solidification based on the change in the sample cooling rate (Figures 9(a) and (b)). This is in agreement with the predictions by all of the peritectic equations as shown in Table II above.

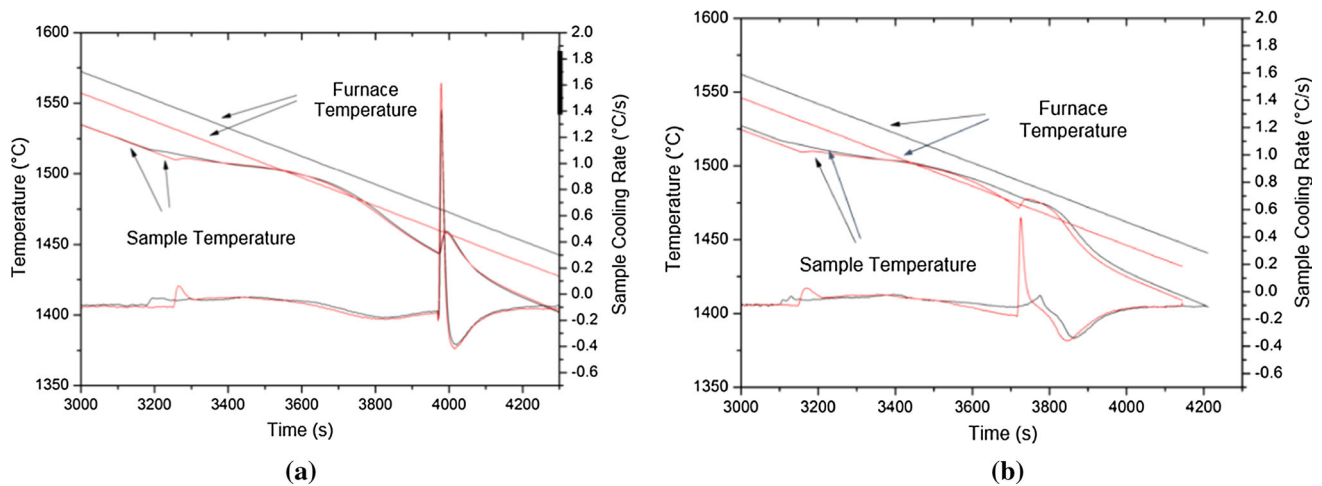


Fig. 4—Thermal analysis results at cooling rate of 0.1 °C/s: (a) P sample and (b) NP sample.

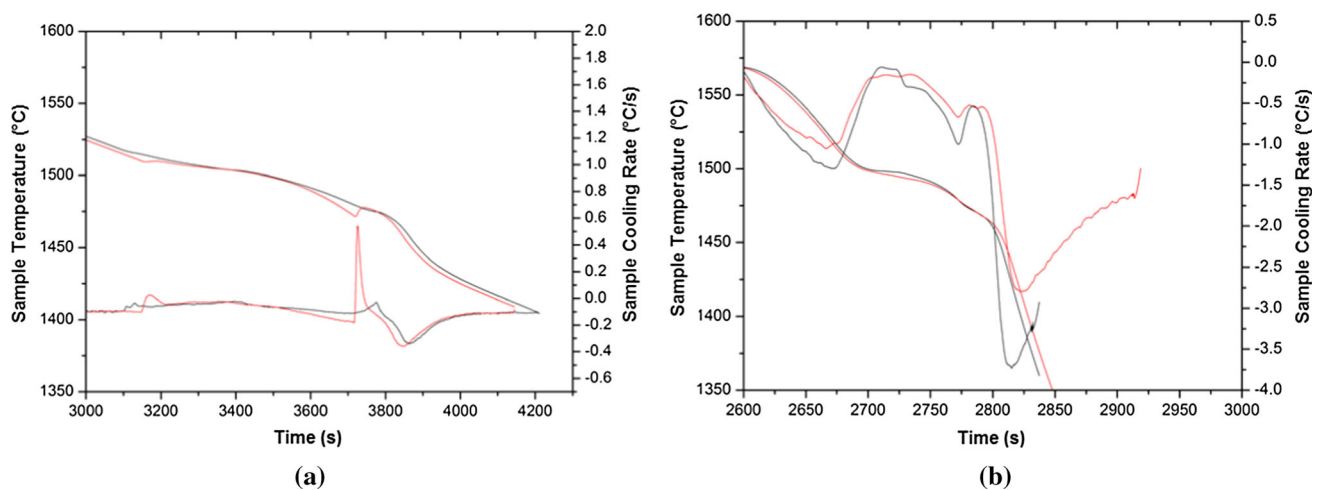


Fig. 5—Thermal analysis results of NP sample: (a) cooling rate: 0.1 °C/s and (b) cooling rate: 1.5 °C/s.

Table III. Peritectic Calculations for Sample NP + Mo

Sample	Kagawa and Okamoto		Blazek <i>et al.</i>		Wolf		Abraham	
	C Range (Pct)	Peritectic (Y/N)	C Range (Pct)	Peritectic (Y/N)	Ferrite Potential Index	Peritectic (Y/N)	Peritectic Potential Index	Peritectic (Y/N)
NP + Mo	0.092 to 0.183	Y	0.074 to 0.183	Y	0.95	Y	94	Y

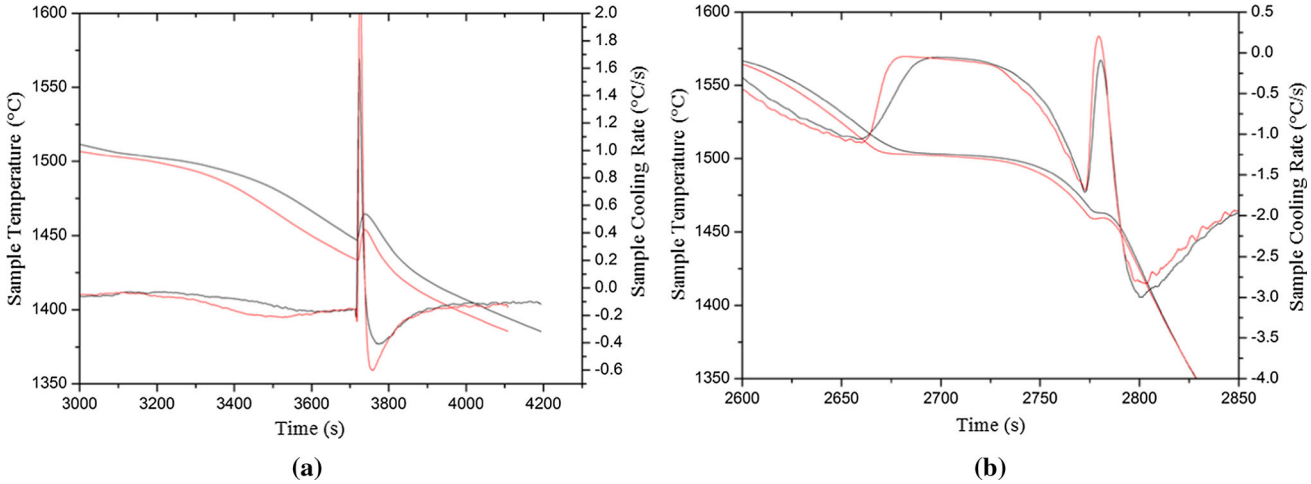


Fig. 6—Thermal analysis results of NP + Mo sample: (a) cooling rate: 0.1 °C/s and (b) cooling rate: 1.5 °C/s.

Table IV. Peritectic Calculations for Sample NP + Si

Sample	Kagawa and Okamoto		Blazek <i>et al.</i>		Wolf		Abraham	
	C Range (Pct)	Peritectic (Y/N)	C Range (Pct)	Peritectic (Y/N)	Ferrite Potential Index	Peritectic (Y/N)	Peritectic Potential Index	Peritectic (Y/N)
NP + Si	0.105 to 0.224	Y	0.065 to 0.161	N	0.89	Y	91	Y

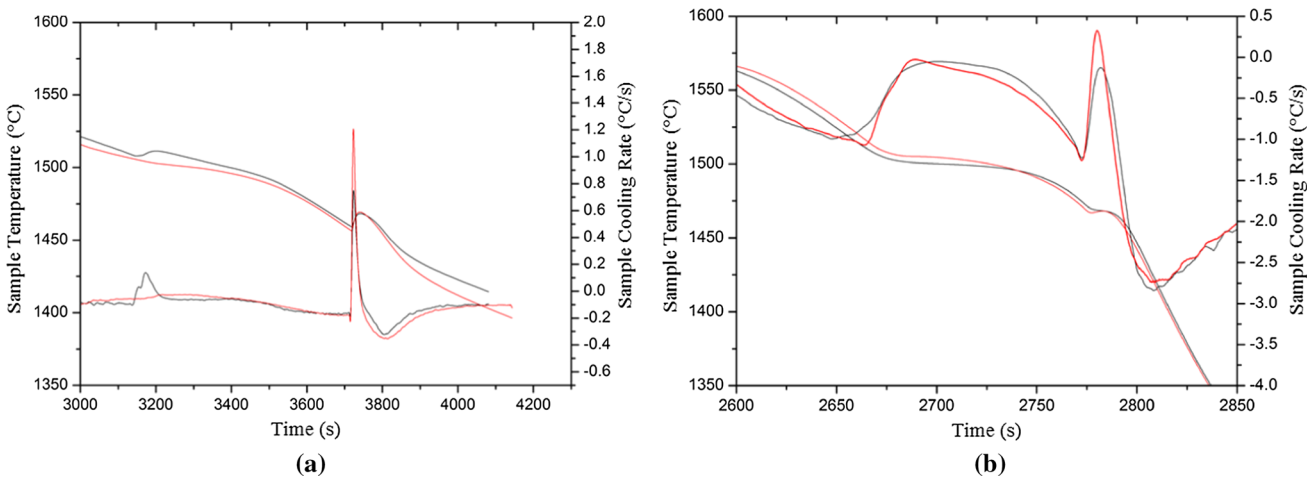


Fig. 7—Thermal analysis results of NP + Si sample: (a) cooling rate: 0.1 °C/s and (b) cooling rate: 1.5 °C/s.

Table V. Peritectic Calculations for Sample NP + Cr

Sample	Kagawa and Okamoto		Blazek <i>et al.</i>		Wolf		Abraham	
	C Range (Pct)	Peritectic (Y/N)	C Range (Pct)	Peritectic (Y/N)	Ferrite Potential Index	Peritectic (Y/N)	Peritectic Potential Index	Peritectic (Y/N)
NP + Cr	0.098 to 0.185	Y	0.066 to 0.166	Y	0.88	Y	85	Y

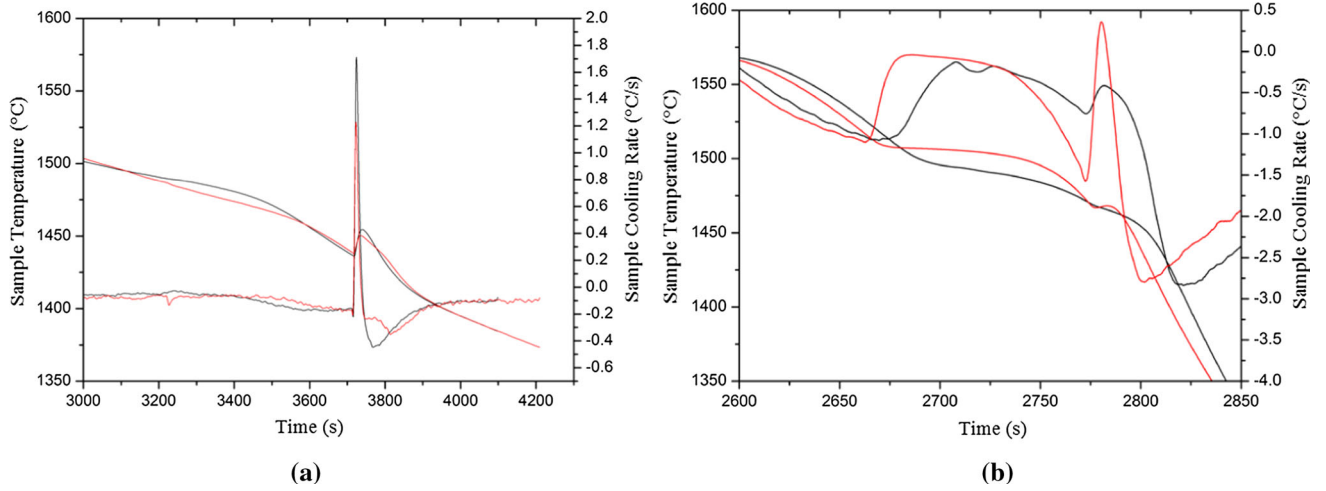


Fig. 8—Thermal analysis results for NP+Cr sample: (a) cooling Rate: 0.1 °C/s and (b) cooling rate: 1.5 °C/s.

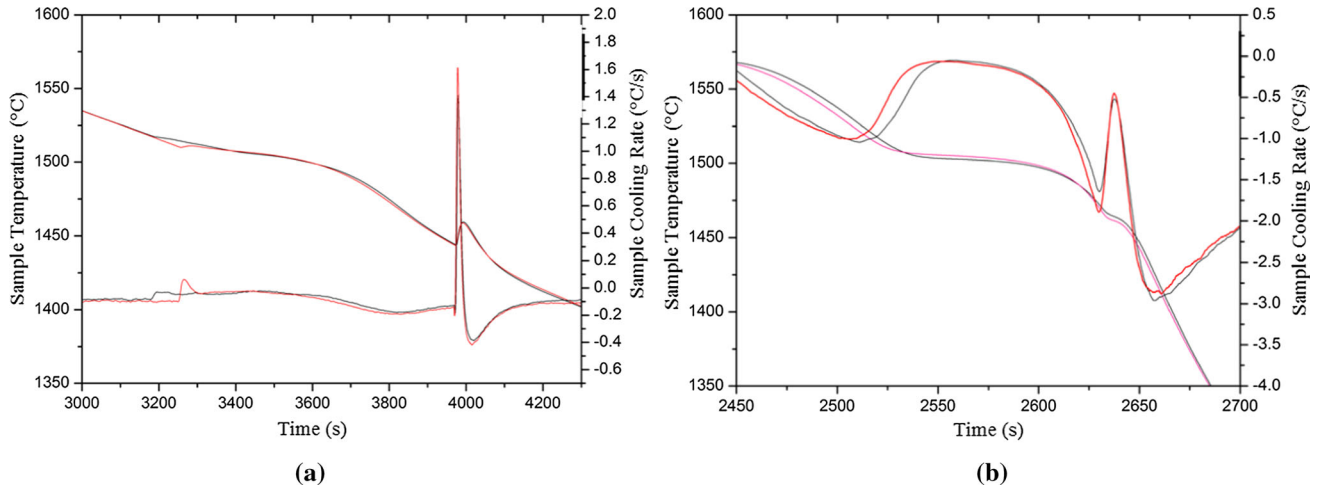


Fig. 9—Thermal analysis results of P sample: (a) cooling rate: 0.1 °C/s and (b) cooling rate: 1.5 °C/s.

Table VI. Predictions by Peritectic Equations for Sample P + Mo

Sample	Kagawa and Okamoto		Blazek <i>et al.</i>		Wolf		Abraham	
	C Range (Pct)	Peritectic (Y/N)	C Range (Pct)	Peritectic (Y/N)	Ferrite Potential Index	Peritectic (Y/N)	Peritectic Potential Index	Peritectic (Y/N)
P + Mo	0.133 to 0.284	N	0.082 to 0.217	Y	1.38	N	40	N

2. Thermal analysis of sample P + Mo

The Mo content in the sample was increased from 0.047 to 1.883 pct. All of the peritectic equations, except that of Blazek *et al.*, predict the steel to be non-peritectic (Table VI). Kagawa & Okamoto's equations show that the carbon content of the steel is below the lower limit of the peritectic range. The equations by Blazek *et al.* show that the carbon content of the steel is well inside the peritectic range. Both Wolf's and Abraham's equations show that the steel is significantly outside peritectic range. Thermal analysis results show that the steel did exhibit peritectic behavior but to a lesser extent compared to the P sample (Figure 10).

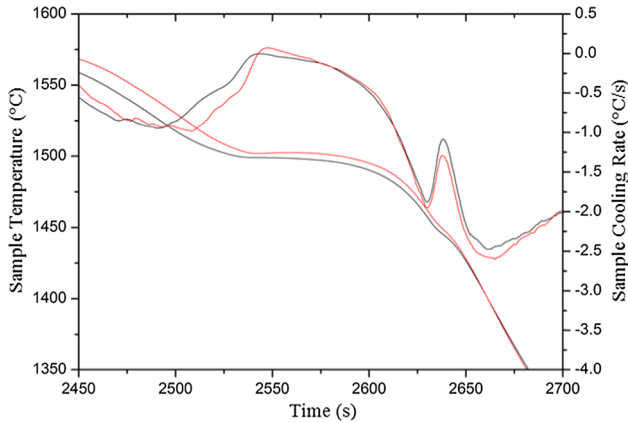


Fig. 10—Thermal analysis results of P + Mo sample (cooling rate: 1.5 °C/s).

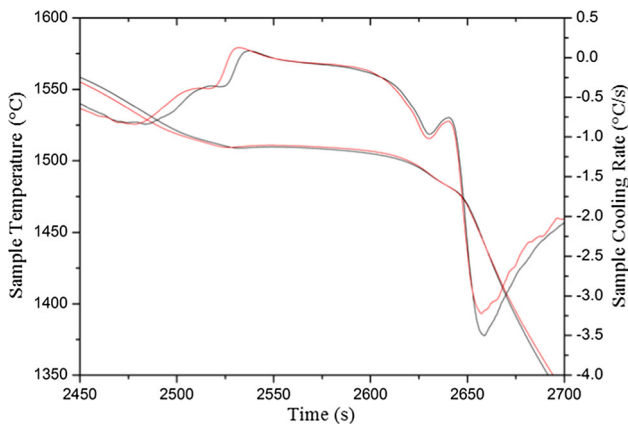


Fig. 11—Thermal analysis results of P - Si sample (cooling rate: 1.5 °C/s).

3. Thermal analysis of sample P - Si

The Si content in the sample was decreased from 0.343 to 0.012 pct. Predictions by all of the peritectic equations, except that of Blazek *et al.*, show that the steel is non-peritectic (Table VII). According to Kagawa & Okamoto's equations, the carbon content of the steel is outside the peritectic range. According to Blazek *et al.*'s equations, the carbon content is well within the peritectic range. According to Wolf's equations, the steel's chemistry is just below the lower peritectic limit, and according to Abraham's equations, the steel is outside the peritectic range. Thermal analysis results show that the steel did not exhibit an appreciable peritectic behavior during solidification (Figure 11).

4. Thermal analysis of sample P - Cr

The Cr content in the sample was decreased from 0.267 to 0.019 pct. All of the peritectic equations, except Abraham's, show that the modified chemistry is well within the peritectic range (Table VIII). Abraham's equations show that the steel just falls below the lower peritectic range. Thermal analysis results show that the steel did not exhibit an appreciable peritectic behavior during solidification (Figure 12).

5. Thermal analysis of sample P-Cr-Si

The Si and Cr contents were decreased from 0.343 pct to 0.093 and from 0.267 pct to 0.106 pct, respectively. The Mo content was maintained at the same level as the P sample. All of the peritectic equations, except Abraham's, predict the steel to be peritectic (Table IX). The equations by Kagawa and Okamoto show the steel's carbon content is just slightly below the upper peritectic range, Blazek *et al.*'s equations show the carbon content is well within the peritectic range, Wolf's equations show that the steel just falls in the peritectic range, and Abraham's equations show the steel is well outside the peritectic range. Thermal analysis results show the steel did not exhibit an appreciable peritectic behavior during solidification (Figure 13).

D. Latent Heat of Peritectic Reaction

The change in latent heat during the peritectic reaction can be used to assess the effect of a change in the concentration of a given solute element on the extent of peritectic reaction. The effects of Mo, Cr, and Si on the peritectic reaction of NP and P steels are summarized in Figures 14 and 15. To illustrate the magnitude of the effect of each element on the peritectic reaction, the thermal analysis curves are overlaid. To quantify the effect of each element, the difference in the peak cooling

Table VII. Predictions by Peritectic Equations for Sample P - Si

Sample	Kagawa and Okamoto		Blazek <i>et al.</i>		Wolf		Abraham	
	C Range (Pct)	Peritectic (Y/N)	C Range (Pct)	Peritectic (Y/N)	Ferrite Potential Index	Peritectic (Y/N)	Peritectic Potential Index	Peritectic (Y/N)
P-Si	0.069 to 0.120	N	0.064 to 0.161	Y	0.82	N	51	N

Table VIII. Predictions by Peritectic Equations for Sample P – Cr

Sample	Kagawa and Okamoto		Blazek <i>et al.</i>		Wolf		Abraham	
	C Range (Pct)	Peritectic (Y/N)	C Range (Pct)	Peritectic (Y/N)	Ferrite Potential Index	Peritectic (Y/N)	Peritectic Potential Index	Peritectic (Y/N)
P-Cr	0.087 to 0.177	Y	0.063 to 0.158	Y	0.91	Y	74	N

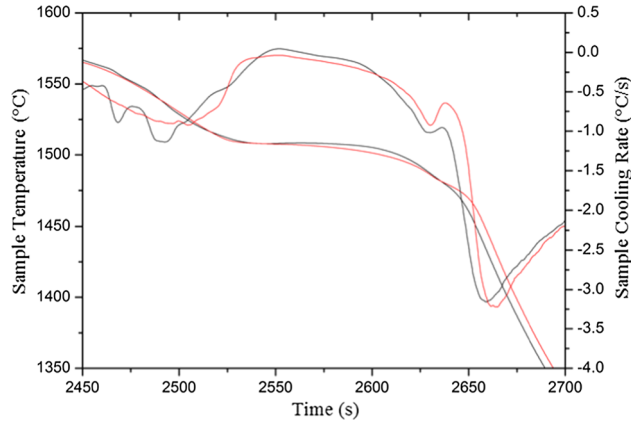


Fig. 12—Thermal analysis results of P – Cr sample (cooling rate: 1.5 °C/s).

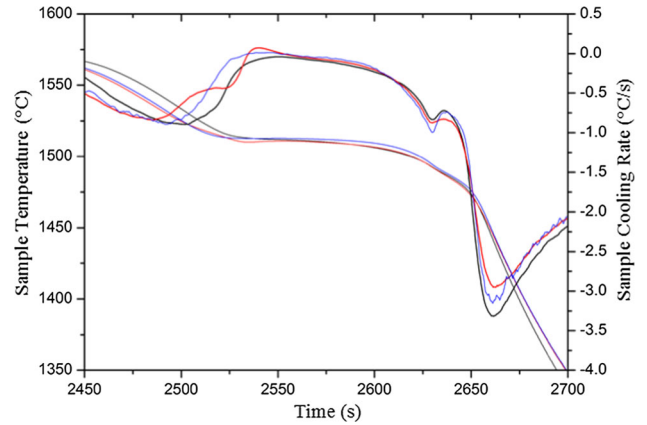


Fig. 13—Thermal analysis results of P-Cr-Si sample (cooling rate: 1.5 °C/s).

rate curve at the peritectic reaction between the base steel and the modified chemistry is used. Therefore, the latent heat of the peritectic reaction can be expressed as follows:

$$\Delta H_p = C_{lFe} M_s (\Delta T_{crm} - \Delta T_{cri}), \quad [2]$$

where ΔH_p is heat of the peritectic reaction in kJ, C_{lFe} is specific heat capacity of iron in the liquid state, M_s is the mass of the sample in kg, ΔT_{crm} is change in sample cooling rate of the modified chemistry, and ΔT_{cri} is the change in sample cooling rate of the NP or P sample. If ΔH_p is positive it means the element increases the peritectic nature of the steel, and if it is negative the element decreases the peritectic nature of the steel.

If expressed per mole, the latent heat takes the form

$$\Delta H_{pmol} = 100 C_{sFe} W_e (\Delta T_{crm} - \Delta T_{cri}) \Delta X^{-1}, \quad [3]$$

where ΔH_{pmol} is the heat of the peritectic reaction per atom, W_e is atomic weight of element in kg, and ΔX is the change in the concentration of solute element in pct.

The values of ΔH_{pmol} for Mo, Si, and Cr for the two steel grades investigated in this study are given in

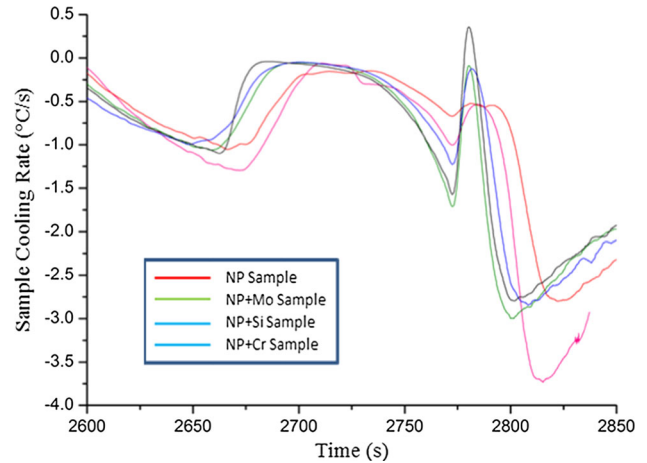


Fig. 14—Comparison of the effect of Si, Cr, and Mo on the peritectic behavior of NP steel (cooling rate: 1.5 °C/s).

Table X. It can be seen that increasing the Mo, or decreasing the Si and Cr contents in the P sample, weaken the peritectic reaction. In the NP sample,

Table IX. Predictions by Peritectic Equations for Sample P-Cr-Si

Sample	Kagawa and Okamoto		Blazek <i>et al.</i>		Wolf		Abraham	
	C Range (Pct)	Peritectic (Y/N)	C Range (Pct)	Peritectic (Y/N)	Ferrite Potential Index	Peritectic (Y/N)	Peritectic Potential Index	Peritectic (Y/N)
P-Si-Cr	0.073 to 0.132	Y	0.065 to 0.161	Y	0.85	Y	39	N

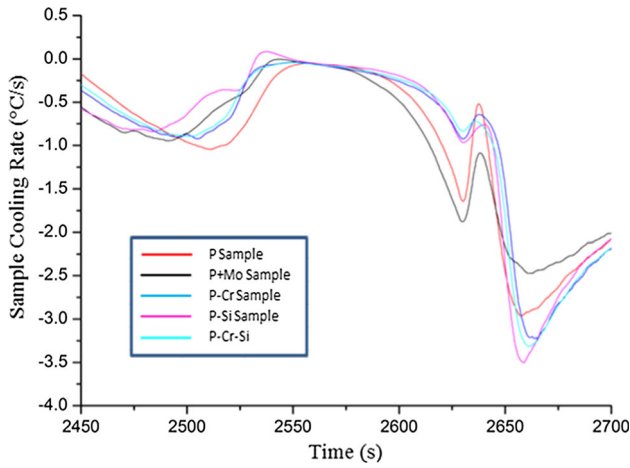


Fig. 15—Comparison of the effect of Si, Cr, and Mo on peritectic behavior of P steel (cooling rate: 1.5 °C/s).

Table X. Latent Heat of Peritectic Reaction

Sample Type	ΔT_{cri}	ΔT_{crm}	ΔH_{pmol}	*Peritectic Behavior
Non-peritectic	0.297			N
Increased Mo		1.629	19.183	E
Increased Si		1.098	5.778	E
Increased Cr		1.917	10.065	E
Peritectic	1.125			P
Increased Mo		0.792	- 1.545	D
Decreased Si		0.207	- 3.466	D
Decreased Cr		0.279	- 7.953	D

*P peritectic, N non-peritectic, D diminished peritectic, E enhanced peritectic.

increasing the Mo, Si, and Cr contents, enhances the peritectic reaction. Note that the values of ΔH_{pmol} given in Table XI for these elements are only for the two base steel grades investigated in this study. Different values are expected for other steel compositions.

E. Thermal Analysis of Low-Carbon Peritectic Steel with Varying Si Content

It is well known in the steel industry that the Si content can affect the peritectic reaction during casting. This is based on the as-cast product surface quality and mold level behavior during casting. Kagawa and Okamoto's equations show a strong effect of Si on the peritectic reaction. In contrast, Blazek *et al.*'s equations

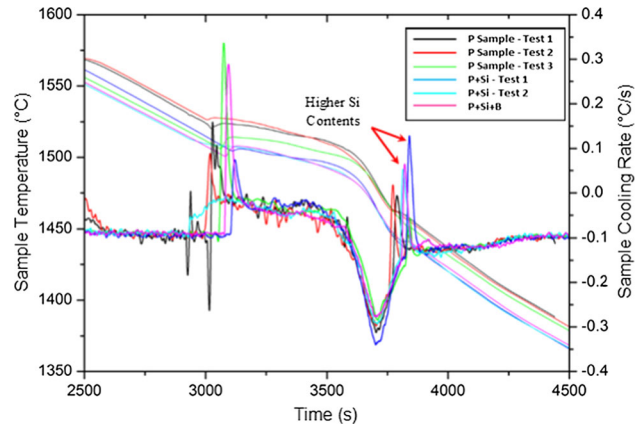


Fig. 16—Thermal analysis results of P steel with modified Si content (cooling rate: 1.5 °C/s).

have a very weak Si effect, probably because the equations were derived for sheet steel chemistries where Si contents are typically very low. Wolf's equations have a moderate Si effect, and Abraham's equations have a very strong Si effect. To further understand the role of Si on the peritectic reaction, thermal analysis experiments were conducted to study the effect of Si on the peritectic behavior of a low-carbon (0.05 pct C) steel by varying its silicon content from 0.15 to 0.33 pct. The results of the thermal analyses and noisy thermocouple readings show that the solidification of the steel was extremely unstable. During the peritectic reaction, the latent heat increased with increased Si content as shown in Figure 16. Peritectic calculations using Abraham's equations predict the steel to be peritectic, and becoming increasingly peritectic as the Si content increases from 0.15 pct to 0.33 pct. Predictions by Wolf's equations show that the steel is peritectic, also becoming increasingly peritectic until the Si content is 0.25 pct. However, at higher Si contents, the steel falls out of the peritectic range. Predictions by Kagawa and Okamoto's equations show that the steel is non-peritectic and with increasing Si content the steel increasingly becomes non-peritectic. Predictions by Blazek *et al.*'s equations show the steel to be only about 0.005 pct C below the lower limit of the peritectic range. With increasing Si content, the steel remains non-peritectic, but the lower carbon limit of the peritectic range gradually decreases. Industrial experience shows that the incidence of surface defects for this grade increases with increasing Si content. The rate of surface defects in as-cast slabs of this steel correlates fairly well with the peritectic potential index proposed

Table XI. Solid Volume Fraction During Peritectic Reaction at Cooling Rate of 1.5 °C/s

Sample	Liquidus Temperature (°C)	Peritectic Start Temperature (°C)	Solidus Temperature (°C)	t_{sol} (s)	K (kg/s ^{1/2}) X10 ⁻²	t_{peri} (s)	f_{sol}
P	1524	1468	1428	64.0	1.00	37.3	0.76
P + Cr	1527	1486	1438	59.3	1.04	27.3	0.68
P + Si	1533	1490	1446	58.0	1.05	28.7	0.70
P + Mo	1524	1455	1400	82.7	0.88	46.0	0.75
P-Si-Cr	1532	1494	1447	56.7	1.06	25.3	0.67

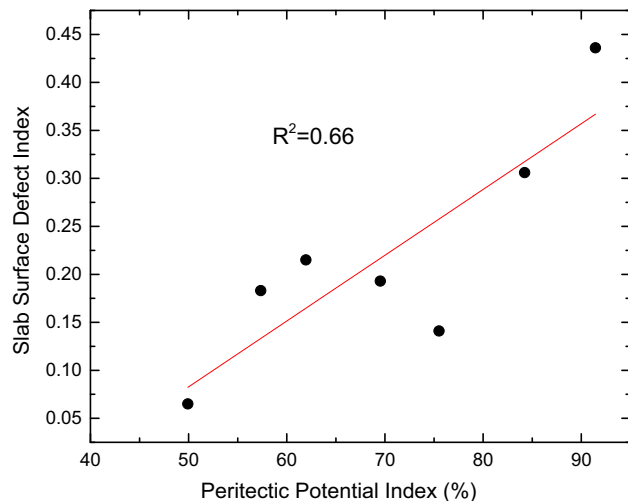


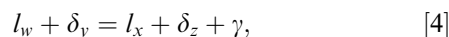
Fig. 17—Correlation of surface defect rate in as-cast slabs to peritectic potential index.

by Abraham as depicted in Figure 17.^[36] Overall, as shown in this paper, all of the peritectic equations are capable of determining the peritectic nature of Fe-C steel, albeit with varying degree of strength. Therefore, it is important to not rely on just one equation when studying the peritectic behavior of steel.

IV. DISCUSSION

Considering the influence of alloying elements, it can be surmised that the solidification path of most steel grades with carbon contents of up to 0.53 pct passes through the peritectic region as demonstrated by pseudo Fe-C phase diagrams.^[33,37] However, the intensity of the peritectic reaction varies depending on where the carbon content of the steel is in relation to the carbon range for the peritectic reaction. In addition, the intensity of the peritectic reaction is also affected by casting conditions. Griesser *et al.*^[40] demonstrated the impact of nucleation undercooling on the mechanism and kinetics of the peritectic phase transition in steel. Their results show that higher cooling rates result in higher undercooling, which in turn increases the driving forces for the peritectic reaction and peritectic transformation. A similar effect of undercooling on the rate of peritectic reaction and solidification structure has been reported by others.^[10,25,41] Therefore, the peritectic reaction in steel with mild peritectic behavior under normal casting conditions should intensify when undercooled.

The peritectic reaction can be written according to Eq. [4].



where l is liquid, δ is delta ferrite, and γ is austenite. Note that the subscripts are intended to indicate different quantity of the phases ($l_w > l_x$ and $\delta_y > \delta_z$).

From the observations by Griesser *et al.*, and Eq. [4], it can be seen that the intensity of the peritectic reaction depends on the proportions of liquid and delta ferrite at

the time of the reaction. If there is no appreciable liquid or delta ferrite, the magnitude of the peritectic reaction will be small and its impact on the quality of the cast product should be negligible. Thus, the magnitude of the peritectic reaction in a given steel depends on the relative position of the steel between the hypoperitectic and hyperperitectic points of the Fe-C diagram.

From the experiments conducted in this study, the liquidus temperatures, peritectic start temperatures, and solidus temperatures were determined for the P and NP samples. The results are summarized in Tables XI, XII, and XIII. Based on the determined temperatures and the cooling rates, the time required for complete solidification (t_{sol}) and the elapsed time before the start of peritectic reaction (t_{peri}) can be calculated using the solidification equation (Eq. [5]).^[42]

$$S = Kt^{1/2}, \quad [5]$$

where S is shell thickness, K is solidification constant, and t is time.

By replacing S with M (mass of steel that solidifies), Eq. [5] takes the form of Eq. [6].

$$M = Kt^{1/2} \quad [6]$$

From the difference between the liquidus and solidus temperatures, t_{sol} can be calculated for 0.080 kg samples used in the experiments. Since M and t are known, K can be determined. With the value of K known, t_{peri} can be determined from the difference between the liquidus and peritectic start temperatures. This analysis further makes it possible to determine solid fraction (f_{sol}) at the time of peritectic reaction. The f_{sol} represents the amount of delta ferrite that transformed from the liquid at the time of the peritectic reaction. Hence, the differences between f_{sol} of the P or NP and their modified chemistries can be used to describe delta ferrite stability and perhaps the intensity of the peritectic reaction. If the modified chemistry has a larger f_{sol} , it implies that the modified alloy will undergo a more pronounced peritectic reaction compared to the base alloy. The difference in the f_{sol} between the modified and unmodified alloy is correlated to the change in latent heat per mole of added elements (ΔH_{pmol}) as shown in Figures 18(a) and (b). From these figures, it can be seen that Cr, Si and Mo decrease the peritectic intensity of the P sample and increase the peritectic intensity in the NP sample. As shown in Tables XII and XIII, the peritectic start temperatures for the samples cooled at 1.5 °C/s are much higher than those cooled at 0.1 °C/s. The reason for the higher temperatures in the samples cooled at 1.5 °C/s may be related to recalescence due to undercooling phenomenon.^[43]

V. CONCLUSIONS

The thermal analysis technique was employed to study the effect of different elements on the peritectic nature of steel. The degree to which each element affects the peritectic behavior of the steel was found to be

Table XII. Solid Volume Fraction During Peritectic Reaction at Cooling Rate of 0.1 °C/s

Sample	Liquidus Temperature (°C)	Peritectic Start Temperature (°C)	Solidus Temperature (°C)	t_{sol} (s)	K (kg/s ^{1/2}) X10 ⁻²	t_{peri} (s)	f_{sol}
NP	1518	1481	1458	600	0.33	370	0.79
NP + Mo	1513	1458	1452	610	0.32	550	0.95
NP + Cr	1504	1442	1431	730	0.30	620	0.92
NP + Si	1509	1464	1454	550	0.34	450	0.90

Table XIII. Solid Volume Fraction During Peritectic Reaction at Cooling Rate of 1.5 °C/s

Sample	Liquidus Temperature (°C)	Peritectic Start Temperature (°C)	Solidus Temperature (°C)	t_{sol} (s)	K (kg/s ^{1/2}) × 10 ⁻²	t_{peri} (s)	f_{sol}
NP	1518	1479	1432	57.3	1.06	26	0.67
NP + Mo	1521	1468	1427	62.7	1.01	35.3	0.75
NP + Cr	1516	1471	1426	60.0	1.03	30.0	0.71
NP + Si	1518	1471	1419	66.0	0.98	31.3	0.69

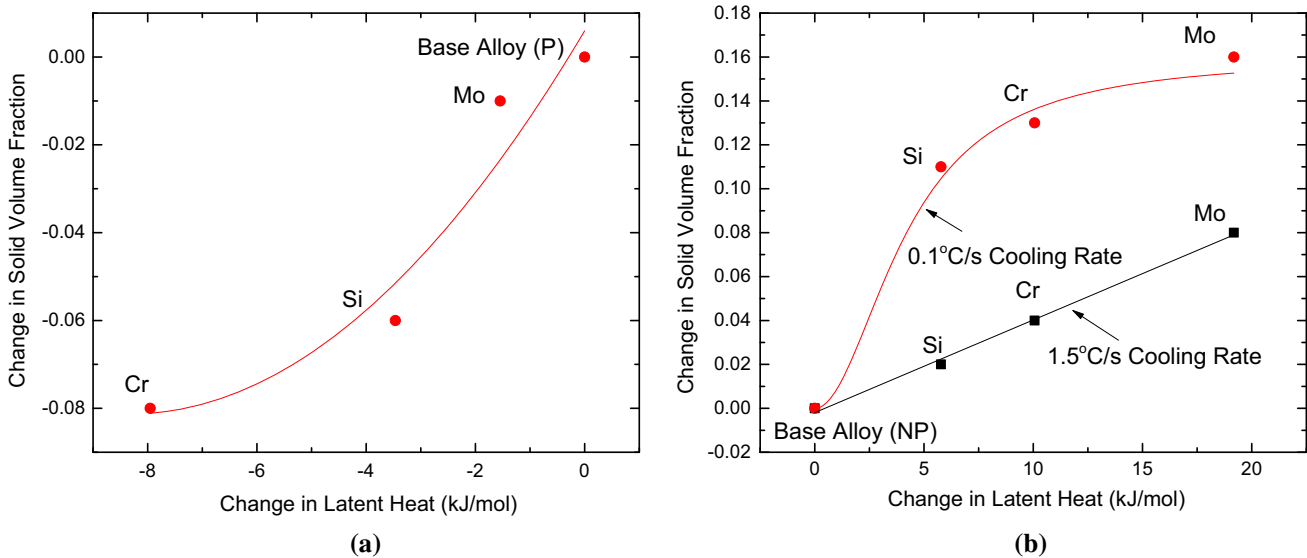


Fig. 18—Effect of alloying elements on volume fraction solid and latent heat during peritectic reaction: (a) peritectic steel and its modifications and (b) non-peritectic steel and its modifications.

proportional to the change in sample cooling rate at the time of the peritectic reaction. The change in sample cooling rate was compared to the predictive power of four peritectic equations. Although there are differences in the predictions by the equations for the chemistries investigated, all the equations demonstrate adequate capability of determining the peritectic nature of the steel. However, because the individual equations do not have the same predictive power for all dissolved elements, it is important to not rely on just one equation for predicting the peritectic behavior of steel during alloy development. From the thermal analysis results, an expression was derived for calculating the heat liberated during the peritectic reaction based on the change in sample cooling rate and change in the concentration of a

given solute element. The change in the heat liberated during the peritectic reaction due to a change in the concentration of a given solute element correlates well with the change in the solid volume fraction at the time of the reaction.

ACKNOWLEDGMENTS

The authors would like to thank Steve Hansen and other SSAB senior managers for supporting this project. Special thanks to Miles Haberkorn and Josh Cottrell for their assistance in this work.

REFERENCES

1. H.W. Kerr and W. Kurz: *Int. Mater. Rev.*, 1996, vol. 41 (4), pp. 132–64.
2. C. Bernhard: *Berg Huettenmännische Monatshefte*, 2004, vol. 149, pp. 90–95.
3. M.M. Wolf: *Ironmak. Steelmak.*, 1986, vol. 13, pp. 248–57.
4. M. Wolf and W. Kurz: *Metall. Trans. B*, 1981, vol. 12B, pp. 85–93.
5. D.H. StJohn: *Acta Metall. Mater.*, 1990, vol. 38 (4), pp. 631–36.
6. D.H. StJohn and L.M. Hogan: *Acta Metall.*, 1987, vol. 35 (1), pp. 171–74.
7. H. Fredriksson and T. Nylén: *Met. Sci.*, 1982, vol. 16, pp. 283–94.
8. D.R. Uhlmann and G.A. Chadwick: *Acta Metall.*, 1961, vol. 9, pp. 835–40.
9. D.H. St. John and L.M. Hogan: *J. Mater. Sci.*, 1982, vol. 17, pp. 2413–18.
10. N.J. McDonald and S. Sridhar: *Metall. Mater. Trans. A*, 2003, vol. 34A, pp. 1931–40.
11. Y.K. Chuang, D. Reinisch, and K. Schwardfeger: *Metall. Trans. A*, 1975, vol. 6A, pp. 235–38.
12. M. M. Wolf: *Steelmaking Conference Proceedings*, ISS-AIME, 1998, pp. 53–61.
13. H. W. Kerr, J. Cisse, and G. F. Bolling: *Acta Metall.*, 1974, pp. 677–86.
14. D.M. Stefanescu: *ISIJ Int.*, 2006, vol. 46 (6), pp. 786–94.
15. J.J.R. Mondragón, M.H. Trejo, M.J.C. Román, and H. Solist: *ISIJ Int.*, 2008, vol. 48 (4), pp. 454–60.
16. A. D. Pitts-Duncan: Particle Engulfment and Pushing by Peritectic Systems, Thesis, 2006, The University of Alabama, Tuscaloosa, U.S.A.
17. A. Grill and J.K. Brimacombe: *Ironmak. Steelmak.*, 1976, vol. 2, pp. 76–79.
18. T. Emi and H. Fredriksson: *MaterSci. Eng. A*, 2005, vol. 413 (414), pp. 2–9.
19. J.S. Lee, S.G. Kim, W.T. Kim, and T. Suzuki: *ISIJ Int.*, 1999, vol. 39 (7), pp. 730–36.
20. J. Tiaden: *J. Cryst. Growth*, 1999, vol. 198/199, pp. 1275–80.
21. M. El-Bealy and H. Fredriksson: *Metall. Mater. Trans. B*, 1996, vol. 27B, pp. 999–1014.
22. H. Nassar and H. Fredriksson: *Metall. Mater. Trans. A*, 2010, vol. 41A, pp. 2776–83.
23. J.E. Rodriguez and D.M. Matson: *Acta Mater.*, 2017, vol. 129, pp. 408–14.
24. H. Shibata, Y. Arai, M. Suzuki, and T. Emi: *Metall. Mater. Trans. B*, 2000, vol. 31B, pp. 981–91.
25. K. Matsuura, H. Maruyama, Y. Itoh, M. Kudoh, and K. Ishii: *ISIJ Int.*, 1995, vol. 35 (2), pp. 183–87.
26. K. Matsuura, Y. Itoh, and T. Narita: *ISIJ Int.*, 1993, vol. 33 (35), pp. 583–87.
27. H. Yasuda, I. Ohnaka, Y. Matsunaga, and Y. Shiohara: *J. Cryst. Growth*, 1996, vol. 158, pp. 128–35.
28. S. Moon: The Peritectic Phase Transition and Continuous Casting Practice, Thesis, 2015, University of Wollongong, Wollongong, Australia.
29. K. Hechu, C. Slater, B. Santillana and S. Sridhar: The 2nd International Symposium on the Recent Developments in Plate Steels, AIST, 2018, pp. 33–42.
30. J. Konishi: Modeling of The Formation of Longitudinal Facial Cracks in Continuous Casting of Steel Slabs, Thesis, 1996, University of British Columbia, Vancouver, Canada.
31. K. Ishida, H. Fukai, H. Ohotani, and K. Nishizawa: *J. Iron Steel Inst. Jpn*, 1985, vol. 71, p. S198.
32. K. Yasumoro, T. Nagamichi, Y. Maehara, and K. Gunji: *J. Iron Steel Inst. Jpn*, 1987, vol. 73, pp. 1738–45.
33. A. S. Normanton, V. Ludlow, A. W. Smith, A. Gotti, M. Thiemann, S. Landa, and J. Wans: Improving Surface Quality of ContinTech. Steel Res., EUR21340 EN, 2005.
34. A. Kagawa and T. Okamoto: *Mater. Sci. Technol.*, 1986, vol. 2, pp. 998–1008.
35. K.E. Blazek, O. Lanzi III, P. L. Gano, and D. L. Kellogg: *AIST Trans. Iron Steel Technol.* 2008, pp. 80–85.
36. S. Abraham: *AIST Trans. Iron Steel Technol.*, 2016, vol. 13 (1), pp. 176–87.
37. B. Carlsson and B. Callmer: *A Guide to the Solidification of Steels*, Södertälje, Jernkontoret, Sweden, Ljungberg Tryckeri AB, 1977, pp. 13–162.
38. P. Presoly, R. Pierer, and C. Bernhard: *Metall. Mater. Trans. A*, 2013, vol. 44A, pp. 5377–88.
39. B.K. Dhindaw, T. Antonsson, J. Tinoco, and H. Fredriksson: *Metall. Mater. Trans. A*, 2004, vol. 35A, pp. 2869–79.
40. S. Griesser, C. Bernhard, and R. Dippenaar: *Acta Mater.*, 2014, vol. 81, pp. 111–20.
41. G.S. Reddy and J.A. Sekhar: *Acta Metall.*, 1989, vol. 37 (5), pp. 1509–19.
42. E.S. Szekeres: *Brimacombe Contin. Cast. Course*, 2000, vol. 2, pp. P1–P5.
43. C.G. Levi and R. Mehrabian: *Met. Trans. A*, 1982, vol. 13A, pp. 221–34.

Publisher's Note Springer Nature remains neutral with regard to jurisdictional claims in published maps and institutional affiliations.